

3D-SIMULATION OF NONLINEAR DYNAMICS FOR A REENTRY VEHICLE

Norihiro Goto^{*}, Takashi Kawakita⁺
 Kyushu University, Fukuoka 812-8581, Japan
 E-mail : goto@aero.kyushu-u.ac.jp

Keywords : *nonlinear dynamics, bifurcation analysis, 3D-simulation*

Abstract

The paper conducts a study of nonlinear aircraft dynamics by means of bifurcation analyses and 3-dimensional visual simulations. A model reentry vehicle is subjected to the study to show that jump phenomena concerning inertial coupling can occur over a wide range of control surface angles, and the basic solution branch is often unstable around a desired level flight equilibrium point. Visual simulations help to understand the vehicle's nonlinear flight dynamics as well as various response characteristics to control inputs associated with its peculiar configuration. Drawing on the study, the paper finally proposes the works to be undertaken in the future.

1 Introduction

It is common practice to design aircraft flight control systems (AFCSs) based on linear models about equilibrium (trim) points. There exist, however, intrinsically nonlinear problems that must be addressed in detail before an aircraft is put into operation inasmuch as it is difficult to recover the original flight condition once it falls into such a problem. Such problems include inertial coupling, which has been known since

around 1948[1]. It is essentially a gyroscopic effect, occurring in high roll-rate maneuvers of modern high speed aircraft including spinning missiles designed in such a way that most of their masses are concentrated in fuselages. For such an aircraft, a slight deviation of its control surface angle from the steady state angle may lead to a drastic change in roll-rate, causing damages on its empennage; known as jump phenomenon. Nonlinear analyses to elucidate this problem have been reported in Refs.2 and 3, for example. However, the aircraft treated in these works are stable around the equilibrium point of level flight. On the other hand, an unstable aircraft combined with malfunctions of AFCSs may result in a catastrophe if it falls into a high roll-rate motion. With this background in mind, the paper's objective is to better understand the problem of inertial coupling by means of bifurcation analyses and three-dimensional (3D) visual simulations.

For this objective, a model reentry vehicle is subjected to analyses. The model vehicle is the Automatic Landing Flight Experiment (ALFLEX) plane[4] as shown in Fig.1, which is a scale model of an unmanned reusable orbiting spacecraft. The ALFLEX plane is a glider having no propulsive means aimed at evaluating the flight characteristics of the spacecraft during final approaches and landing phases. Its stable flight is made possible with the help of elaborate AFCSs, without which the bare configuration is unstable both longitudinally and lateral-directionally over a wide speed range.

* Professor, Department of Aeronautics and Astronautics. Associate Fellow AIAA.

+ Graduate Student, Department of Aeronautics and Astronautics.

Such characteristics of the ALFLEX plane make it important to look into the trimmability of the bare vehicle in case a malfunction of AFCSs should occur.

The paper first conducts bifurcation analyses combined with the stability analyses of the equilibrium branches. Based on the result of the analyses, 3D visual simulations are conducted of the vehicle's dynamic nonlinear flights. It is shown that visual simulations help to better understand the vehicle's nonlinear phenomena related to inertial coupling as well as various response characteristics to control inputs associated with its peculiar configuration. Drawing on these studies, the paper finally proposes works to be undertaken in the future.

2 Equations of Motion

Because high roll-rate steady states are of primary concern here, the original six degrees of freedom equations of motion of a rigid aircraft with respect to an xyz body-axis system[5], where xz is the plane of symmetry, are reduced to five degrees of freedom ones under the assumptions,

1) forward velocity V , weight W , and air density ρ are constant, and

2) angle of attack α and sideslip angle β are small.

The resulting equations of motion are

$$\dot{\beta} = p \sin \alpha - r \cos \alpha + \hat{y} + \frac{g}{V} \sin \phi \cos \theta \quad (1)$$

$$\dot{\alpha} = -p \beta + q + \hat{z} + \frac{g}{V} \cos \phi \cos \theta \quad (2)$$

$$\dot{p} - \frac{I_{xz}}{I_x} \dot{r} = i_1 (-qr + i_a pq + \hat{l}) \quad (3)$$

$$\dot{q} = i_2 (rp + i_b (-p^2 + r^2) + \hat{m}) \quad (4)$$

$$\dot{r} - \frac{I_{xz}}{I_z} \dot{p} = i_3 (-pq - i_c qr + \hat{n}) \quad (5)$$

where the Eulerian angles, roll angle ϕ and pitch angle θ , are determined by the kinematic relations as

$$\dot{\phi} = p + q \sin \phi \tan \theta + r \cos \phi \tan \theta \quad (6)$$

$$\dot{\theta} = q \cos \phi - r \sin \phi \quad (7)$$

In Eqs.(1)~(7)

$$\begin{aligned} i_1 &= \frac{I_z - I_y}{I_x}, \quad i_2 = \frac{I_z - I_x}{I_y}, \quad i_3 = \frac{I_y - I_x}{I_z}, \\ i_a &= \frac{1}{i_1} \frac{I_{xz}}{I_x}, \quad i_b = \frac{1}{i_2} \frac{I_{xz}}{I_y}, \quad i_c = \frac{1}{i_3} \frac{I_{xz}}{I_z}, \\ \hat{y} &= \frac{g}{WV} Y_a, \quad \hat{z} = \frac{g}{WV} Z_a, \\ \hat{l} &= \frac{L}{i_1 I_x}, \quad \hat{m} = \frac{M}{i_2 I_y}, \quad \hat{n} = \frac{N}{i_3 I_z} \end{aligned} \quad (8)$$

I_x, I_y, I_z : moments of inertia about x -, y -, and z -axis, respectively,

I_{xz} : product of inertia,

Y_a, Z_a : aerodynamic forces,

L, M, N : aerodynamic moments about the center of gravity,

p, q, r : angular velocities about x -, y -, and z -axis, respectively,

g : gravitational acceleration.

Among the inertial parameters in Eq.(8), i_3 is referred to as the inertial coupling parameter. It can be learned from Eq.(5) that a large value of i_3 produces large inertial coupling moments. In comparison with the data given in Ref.1, the ALFLEX plane, of which the dimensional data are given in Table1, has the same magnitude of i_3 as that of the F100A fighter plane which suffered from an inertial coupling problem in its early phase of development.

Aerodynamic forces and moments in Eqs.(1)~(5) are assumed here to be linearly related to motion variables and control surface angles mainly because of lack of nonlinear aerodynamic data. Table1 summarizes the linear relationships and numerical data necessary for the analysis to follow. The reader is referred to Ref.6 for an example of complete treatment of nonlinear aerodynamic data. Note in Table1 that a level flight with the steady state pitch angle θ_0

and angle of attack α_0 is a trivial trim point. Those original equations of motion, Eqs.(1)~(7), can be represented by the general form as

$$\dot{\mathbf{x}} = \mathbf{H}(\mathbf{x}, \boldsymbol{\delta}) \quad (9)$$

where

$$\mathbf{x} = [\beta, \alpha, p, q, r, \phi, \theta]^T \quad (10)$$

$$\boldsymbol{\delta} = [\delta_e, \delta_a, \delta_r]^T, \quad (11)$$

and δ_e : elevator angle, δ_a : aileron angle, δ_r : rudder angle.

General trim points are determined by solving the transcendental algebraic equation

$$\mathbf{H}(\mathbf{x}, \boldsymbol{\delta}) = 0 \quad (12)$$

The vehicle, however, cannot attain all of the trim points obtained from Eq.(12). If it has unstable dynamics in the neighborhood of a trim point, a slight external disturbance or a slight deviation of control surface angles from their precise values at the trim point cannot allow the vehicle to stay at the trim point. Stability of the vehicle's dynamics in the neighborhood of a trim point must be examined in order to know whether or not a steady state can be actually attained. To this end, the stability analysis of trim points is made by using the Lyapunov's first method[7], in which the nonlinear equations of motion, Eqs.(1)~(5), are linearized about a trim point as

$$\dot{\mathbf{x}}_\varepsilon = \mathbf{F}\mathbf{x}_\varepsilon \quad (13)$$

where

$\mathbf{x}_\varepsilon = [\beta_\varepsilon, \alpha_\varepsilon, p_\varepsilon, q_\varepsilon, r_\varepsilon]^T$: perturbed variable vector,

and \mathbf{F} is the Jacobian matrix explicitly given by:

$$\mathbf{F} = \begin{bmatrix} \hat{y}_\beta & \bar{p} & \bar{\alpha} + \sin \alpha_0 \\ -\bar{p} & \hat{z}_\alpha & -\bar{\beta} \\ i_p(\hat{l}_\beta / i_a + i_3 \hat{n}_\beta) & 0 & i_p[(1 - i_3)\bar{q} \\ & & + (\hat{l}_p / i_a + i_3 \hat{n}_p)] \\ 0 & i_2 \hat{m}_\alpha & i_2(\bar{r} - 2i_b \bar{p}) \\ i_r(i_1 \hat{l}_\beta + \hat{n}_\beta / i_c) & 0 & i_r[(i_1 i_a - 1 / i_c)\bar{q} \\ & & + (i_1 \hat{l}_p + \hat{n}_p / i_c)] \\ 0 & \hat{y}_r - \cos \alpha_0 & \\ 1 & 0 & \\ i_p[(1 - i_3)\bar{p} & i_p[-(1 / i_a + i_3 i_c)\bar{q} \\ - (1 / i_a + i_3 i_c)\bar{r}] & + (\hat{l}_r / i_c + i_3 \hat{n}_r)] \\ i_2 \hat{m}_q & i_2(\bar{p} + 2i_b \bar{r}) \\ i_r[(i_1 i_a - 1 / i_c)\bar{p} & i_r[-(i_1 + 1)\bar{q} \\ - (i_1 + 1)\bar{r}] & + (i_1 \hat{l}_r + \hat{n}_r / i_c)] \end{bmatrix} \quad (14)$$

In Eq.(14) stability derivatives \hat{y}_β and so on are defined in Table 1, and $\bar{\alpha}, \bar{\beta}, \bar{p}, \bar{q}$ and \bar{r} denote the steady state values, while

$$i_p = \frac{I_{xz} I_z}{I_x I_z - I_{xz}^2}, \quad i_r = \frac{I_{xz} I_x}{I_x I_z - I_{xz}^2} \quad (15)$$

If all of the eigenvalues of \mathbf{F} have negative real parts, the trim point is asymptotically stable, whereas it is unstable, if some eigenvalues have positive real parts. It sometimes happens that the real parts of some eigenvalues are zero or close to zero, generating so-called bifurcation points. In such a case, it is necessary to consider the effects of nonlinear terms on the behavior of the solution in the neighborhood of the trim point. The center manifold theory can be applied to such a case[7].

3 Bifurcation Analysis

Using the continuation method[3], equilibrium branch analyses are made here followed by the stability analyses of trim points for the flight configuration of Table1. Flight control of the ALFLEX plane actually uses elevator δ_e , aileron δ_a , rudder δ_r , and speed brake δ_s as available control inputs. However, in this

analysis the rudder angle is set equal to zero, and the speed brake is fixed at a certain angle. Therefore, the equilibrium branches are determined by varying δ_e and δ_a as parameters. The ranges of variation are $-10 \sim 10$ deg for $\Delta\delta_e$, which denotes an incremental elevator deflection from the initial value of Table1, and $-20 \sim 20$ deg for δ_a . First of all, the results from the equilibrium branch analyses are shown in Figs.2 and 3, where $\Delta\alpha$ is also an incremental angle of attack. Figures 2(a)~2(e) show the equilibrium branches in the plane of motion variables vs. δ_a for a $\Delta\delta_e$, while Figs.3(a)~3(b) together with Fig.2(b) exhibit the variation of p vs. δ_a equilibrium branches for three kinds of $\Delta\delta_e$. It results from the ensuing stability analyses that the trim points on solid equilibrium branches are stable, whereas those on broken branches are unstable. By numerically integrating the original nonlinear equations of motion, these equilibrium branches with stability information have been validated with an additional finding that the origin of $p - \delta_a$ plane for $\Delta\delta_e = -6$ deg actually yields a limit cycle oscillation. The elevator angle should be smaller than -6 deg in order for the origin to be a stable trim point.

More importantly, the equilibrium branches with stability information thus obtained may tell the combinations of $(\Delta\delta_e, \delta_a)$ for which jump phenomena are likely to occur. For example, assume that the vehicle is in a steady rolling state of about 100 deg/s for a combination of $(\Delta\delta_e, \delta_a) = (4 \text{ deg}, 0 \text{ deg})$ as read from Fig.2(b). A deviation of the aileron angle to 2 deg brings the roll-rate abruptly to about -200 deg/s, because at the new aileron angle the trim point on the same equilibrium branch is not stable any more. Looking at Fig.2(b) again, it can be observed that depending on the combination of $(\Delta\delta_e, \delta_a)$ there exist multiple stable trim points or attractors. An interesting question is to which attractor the motion will converge, given the corresponding combination of control surface angles and an arbitrary set of initial conditions. If

the motion starts from within the region of attraction of an attractor, it will settle down on the attractor. For an arbitrary set of initial conditions, however, a general flow pattern of the solution trajectories needs to be known in the phase plane of seven variables. This question must be pursued further in the future.

4 3D Simulation

A numerical simulation is useful to better understand the flight-dynamical characteristics implicit in the nonlinear equations of motion. Furthermore, it enables one to visualize the vehicle's dynamic motion. 3D simulation software developed in this work uses the Runge-Kutta-Gill method for integrating the nonlinear equations of motion, Eqs.(1)~(7), and the Microsoft Visual C++ 6.0 for visualizing the temporal solutions. Figure4 is a snapshot, as seen from a fixed-point in space, from the visual 3D flight simulation. The vehicle in Fig.4 is close to a steady state for a combination of step inputs of $\Delta\delta_e$ and δ_a . Velocity and angular velocity vectors are shown in the figure as V and ω , respectively, together with the body-fixed three axes, X, Y, and Z. This type of simulation helps to figure out what the steady state motion of rotation is like, while at the same time it points out the defects of the analysis; e.g., in Fig.4 the angle of attack α at this moment is almost 90 deg, violating the assumption that α be small. More realistic analyses should be undertaken, getting rid of the assumptions and using nonlinear aerodynamic data.

A series of figures, Figs.5(a)~5(d), illustrates the mechanism of a reversed roll-response to an aileron input, which takes place at the flight configuration of Table1. An aileron input $\delta_a > 0$ is applied to produce a positive rolling moment (Fig.5(a)). Due to the adverse aileron yaw the vehicle yaws to the left (Fig.5(b)). The negative weather-cock stability ($C_{n\beta} < 0$) makes the heading point further left (Fig.5(c)), while sideslipping to the right. The strong dihedral

effect, due to the vertical fin ($C_{l_\beta} < 0$) reverses the rolling motion, ending up in the direction opposite to the initial tendency (Fig.5(d)). As shown in this example, this 3D visual simulation helps to understand the flight mechanism of a reentry vehicle, which poses interesting flight problems because of its generally unusual configuration.

5 Conclusion

A study of nonlinear aircraft dynamics has been conducted by means of bifurcation analyses and 3D visual simulations. A model reentry vehicle has been subjected to the study to demonstrate that jump phenomena concerning inertial coupling can occur over a wide range of control surface inputs, and the basic solution branch is unstable for certain combinations of control surface angles so that it is difficult to recover the original level steady state flight once it falls into an inertial coupling problem. 3D visual simulations can help to better understand the vehicle's nonlinear flight dynamics, if qualitatively. It is a work for the future to devise a remedy control technique for recovery from a general nonlinear motion for a more realistic case where complete nonlinear equations of motion are utilized together with nonlinear aerodynamic data.

References

- [1] Abzug, M.J. and Larrabee, E.E. : *Airplane Stability and Control. A History of the Technologies That Made Aviation Possible*, Cambridge University Press, Cambridge, U.K., Chap.8, 1997.
- [2] Schy, A.A. and Hannah, M.E., "Prediction of Jump Phenomena in Rolling Coupled Maneuvers of Airplanes", *Journal of Aircraft*, Vol.14, pp.375-382, April 1977.
- [3] Carrol, J.V. and Mehra, R.D., "Bifurcation Analysis of Nonlinear Aircraft Dynamics", *Journal of Guidance, Control, and Dynamics*, Vol.5, No.5, pp.529-536, 1982.
- [4] Miyazawa, Y., Motoda, T., Izumi, T., and Hata, T., "Longitudinal Landing Control Law for an Autonomous Reentry Vehicle", *Journal of Guidance, Control, and Dynamics*, Vol.22, No.6, pp.791-800, 1999.
- [5] Etkin, B. and Reid, L.D. : *Dynamics of Flight - Stability and Control*, 3rd Edition, John Wiley & Sons, N.Y., Chap.4, 1996.
- [6] Sibilski, K., "An Agile Aircraft Non-linear Dynamics by Continuation Methods and Bifurcation Theory", *Proceedings of the 22nd International Congress of Aeronautical Sciences 2000 (CD-ROM)*, Paper No. ICAS-2000-3.11.2, Aug. 2000.
- [7] Khalil, H.K. : *Nonlinear Systems*, Macmillan, N.Y., Chaps.3 and 4, 1992.

Table1 Flight configuration, stability derivatives and numerical data

$$\begin{aligned}\hat{y} &= (g/WV)(1/2\rho V^2 SC_y) = \hat{y}_\beta \beta + \hat{y}_r r + \hat{y}_{\delta_r} \delta_r \\ C_y &= (C_{y_\beta})\beta + (C_{y_r})r + (C_{y_{\delta_r}})\delta_r \\ \hat{z} &= (g/WV)(1/2\rho V^2 SC_z) = \hat{z}_0 + \hat{z}_\alpha \Delta\alpha + \hat{z}_{\delta_e} \Delta\delta_e \\ C_z &= C_{z0} + (C_{z_\alpha})\Delta\alpha + (C_{z_{\delta_e}})\Delta\delta_e \\ C_{z0} &= -W \cos\theta_0 / (1/2\rho V^2 S) \\ C_{z_\alpha} &= -C_{L_\alpha} \cos\alpha_0 + C_L \sin\alpha_0 - C_{D_\alpha} \sin\alpha_0 - C_D \cos\alpha_0 \\ C_{z_{\delta_e}} &= -C_{L_{\delta_e}} \cos\alpha_0 - C_{D_{\delta_e}} \sin\alpha_0 \\ \hat{l} &= (1/2\rho V^2 S b C_l) / (i_1 I_x) = \hat{l}_\beta \beta + \hat{l}_p p + \hat{l}_r r + \hat{l}_{\delta_a} \delta_a + \hat{l}_{\delta_r} \delta_r \\ C_l &= (C_{l_\beta})\beta + (C_{l_p})p + (C_{l_r})r + (C_{l_{\delta_a}})\delta_a + (C_{l_{\delta_r}})\delta_r \\ \hat{m} &= (1/2\rho V^2 S c C_m) / (i_2 I_y) = \hat{m}_\alpha \Delta\alpha + \hat{m}_{\dot{\alpha}} \Delta\dot{\alpha} + \hat{m}_q q + \hat{m}_{\delta_e} \Delta\delta_e \\ C_m &= (C_{m_\alpha})\Delta\alpha + (C_{m_{\dot{\alpha}}})\Delta\dot{\alpha} + (C_{m_q})q + (C_{m_{\delta_e}})\Delta\delta_e \\ \hat{n} &= (1/2\rho V^2 S b C_n) / (i_3 I_z) = \hat{n}_\beta \beta + \hat{n}_p p + \hat{n}_r r + \hat{n}_{\delta_a} \delta_a + \hat{n}_{\delta_r} \delta_r \\ C_n &= (C_{n_\beta})\beta + (C_{n_p})p + (C_{n_r})r + (C_{n_{\delta_a}})\delta_a + (C_{n_{\delta_r}})\delta_r\end{aligned}$$

δ_a : aileron angle, δ_r : rudder angle, $\Delta\delta_e$: incremental elevator angle

$W (N) = 760g$	$V (m/s) = 73.84$
$I_x (kg m^2) = 407$	$\alpha_0 (\text{deg}) = 8.18$
$I_y (kg m^2) = 1366$	$\gamma_0 (\text{deg}) = -17.34$
$I_z (kg m^2) = 1643$	$\theta_0 (\text{deg}) = \gamma_0 + \alpha_0 = -9.16$
$I_{xz} (kg m^2) = 10.4$	$\delta_{e0} (\text{deg}) = 3.0$
$S (m^2) = 9.45$	
$c (m) = 3.154$	$\rho (kg/m^3) = 1.156$
$b (m) = 3.295$	

$C_L = 0.2387$	$C_{L_\alpha} = 2.016$	$C_{L_{\delta_e}} = 0.6355$		
$C_D = 0.0745$	$C_{D_\alpha} = 0.2714$	$C_{D_{\delta_e}} = 0.1019$		
$C_{m_\alpha} = -0.0134$	$C_{m_q} = -0.0474$	$C_{m_{\delta_e}} = -0.2152$		
$C_{y_\beta} = -0.6849$	$C_{y_{\delta_r}} = 0.1907$			
$C_{l_\beta} = -0.1774$	$C_{l_p} = -0.0070$	$C_{l_r} = 0.0040$	$C_{l_{\delta_a}} = 0.1488$	$C_{l_{\delta_r}} = 0.0788$
$C_{n_\beta} = -0.0657$	$C_{n_p} = 0.0032$	$C_{n_r} = -0.0060$	$C_{n_{\delta_a}} = -0.0266$	$C_{n_{\delta_r}} = -0.0990$

All other derivatives are set equal to zero.

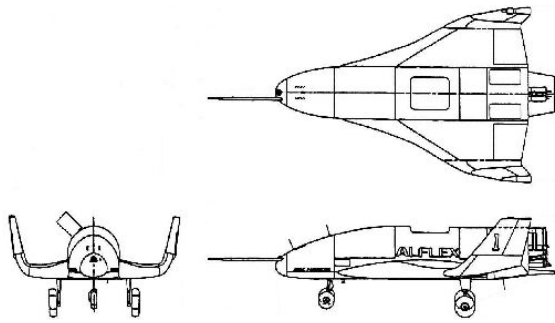


Fig.1 Three views of the ALFLEX plane.

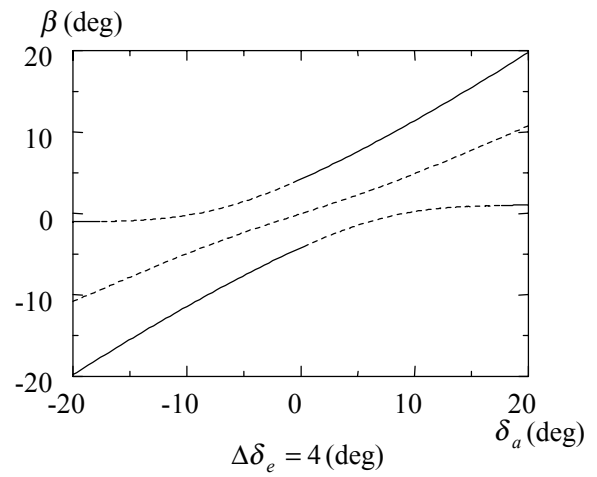


Fig.2(a)

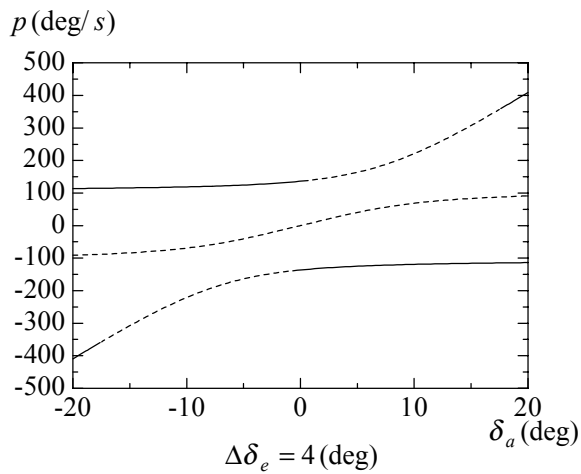


Fig.2(b)

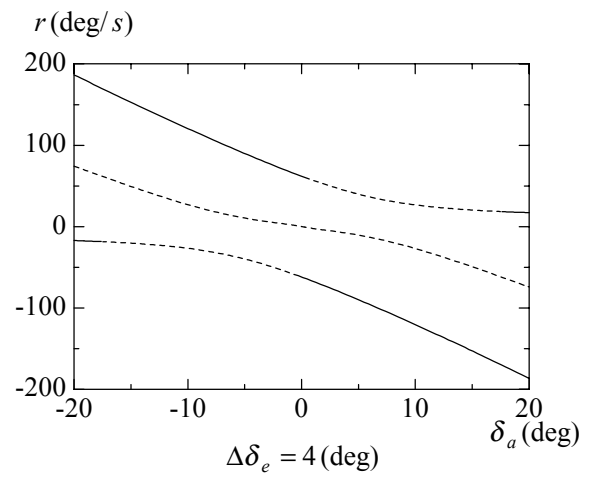


Fig.2(c)

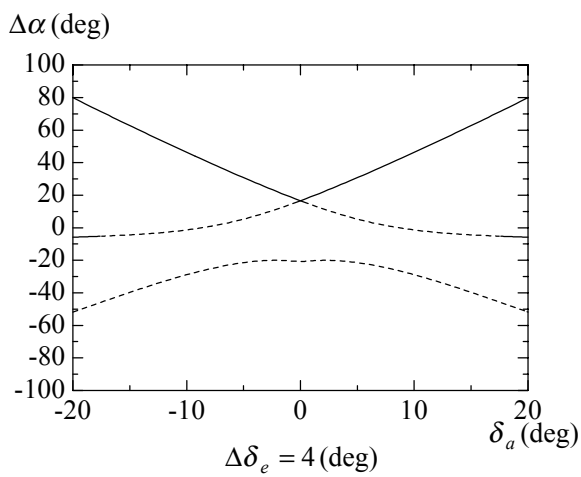


Fig.2(d)

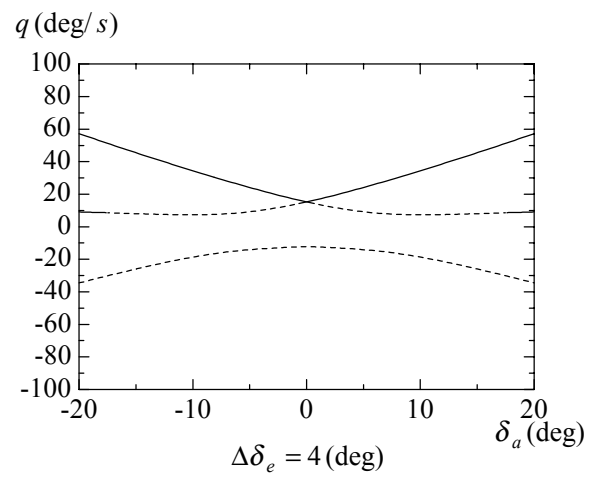


Fig.2(e)

Fig.2 Equilibrium branches of motion variables for $\Delta\delta_e = 4$ deg.

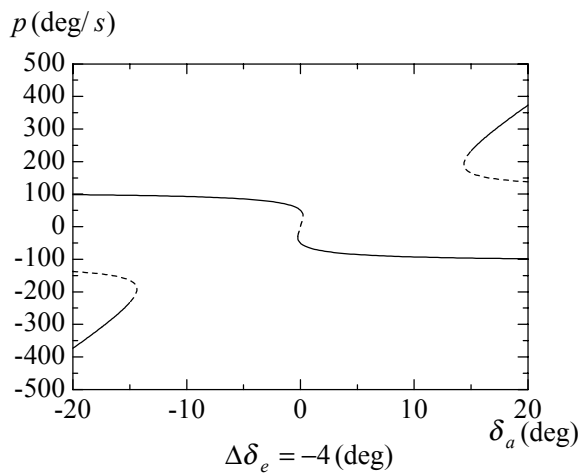


Fig.3(a)

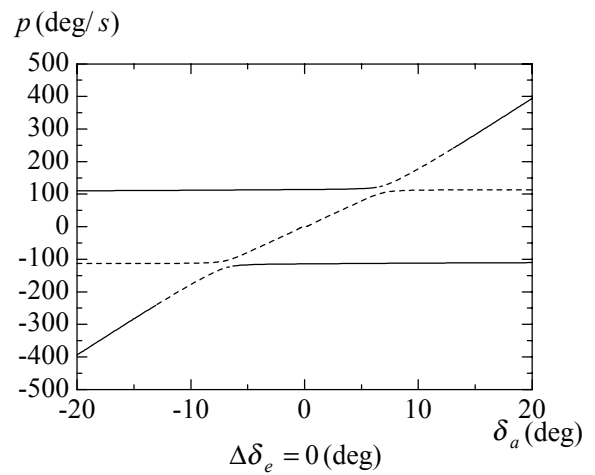


Fig.3(b)

Fig.3 Equilibrium branches of roll-rate for $\Delta\delta_e = -4$ and 0 deg.

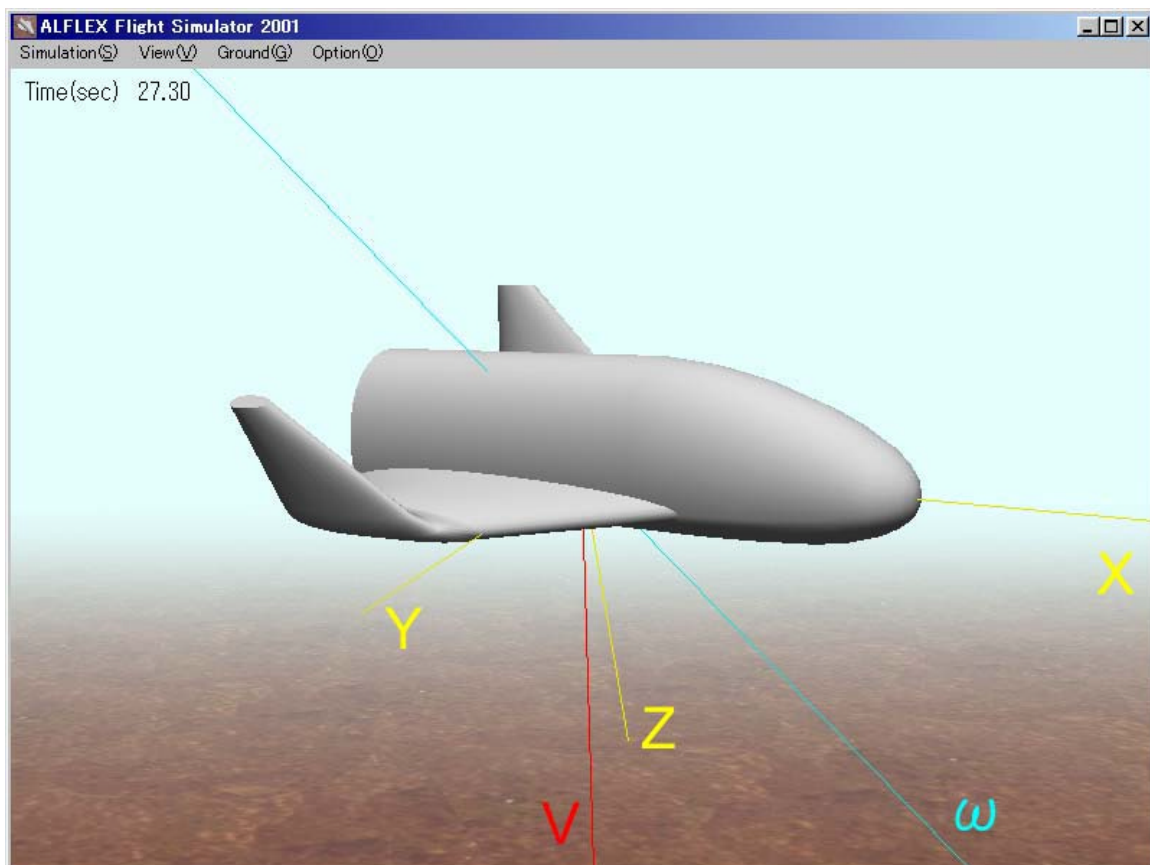


Fig.4 A snap shot of the ALFLEX plane in steady state motion.

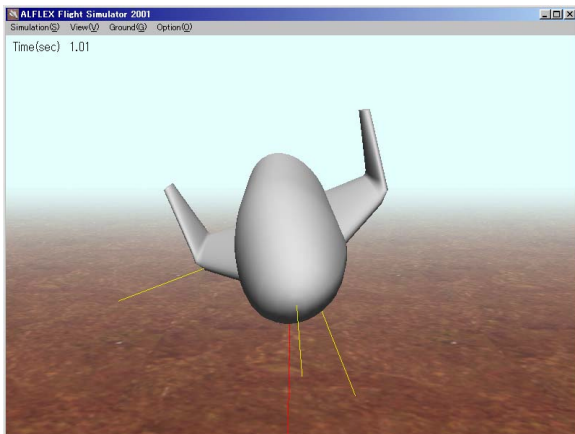


Fig.5(a)

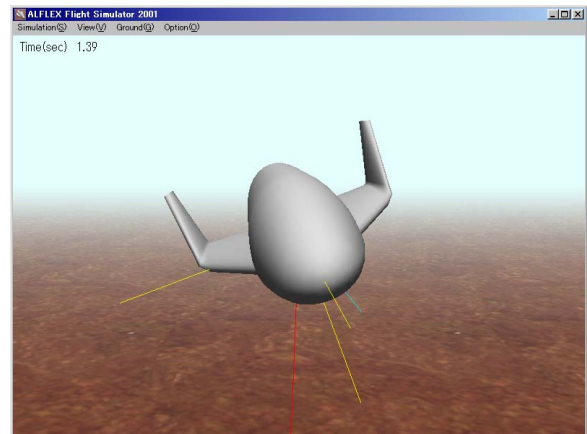


Fig.5(b)

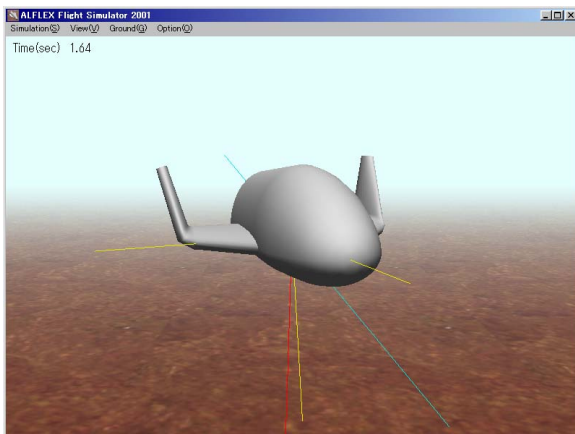


Fig.5(c)

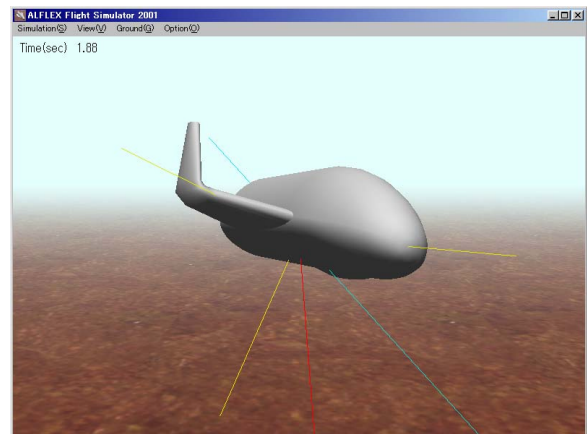


Fig.5(d)

Fig.5 Visual demonstration of a reversed roll-response to an aileron input.